Earth, Planets and Space

FULL PAPER Open Access

The MMX rover: performing in situ surface investigations on Phobos

Patrick Michel[1*†], Stephan Ulamec[2†], Ute Böttger[3], Matthias Grott[4], Naomi Murdoch[5], Pierre Vernazza[6], Cecily Sunday[7], Yun Zhang[1], Rudy Valette[8], Romain Castellani[8], Jens Biele[2], Simon Tardivel[9], Olivier Groussin[6], Laurent Jorda[6], Jörg Knollenberg[4], Jan Thimo Grundmann[10], Denis Arrat[9], Gabriel Pont[9], Stephane Mary[11], Markus Grebenstein[12], Hirdy Miyamoto[13], Tomoki Nakamura[14], Koji Wada[15], Kent Yoshikawa[16] and Kiyoshi Kuramoto[17]

Abstract

The Japanese MMX sample return mission to Phobos by JAXA will carry a rover developed by CNES and DLR that will be deployed on Phobos to perform in situ analysis of the Martian moon's surface properties. Past images of the surface of Phobos show that it is covered by a layer of regolith. However, the mechanical and compositional properties of this regolith are poorly constrained. In particular, from current remote images, very little is known regarding the particle sizes, their chemical composition, the packing density of the regolith as well as other parameters such as friction and cohesion that influence surface dynamics. Understanding the properties and dynamics of the regolith in the low-gravity environment of Phobos is important to trace back its history and surface evolution. Moreover, this information is also important to support the interpretation of data obtained by instruments onboard the main MMX spacecraft, and to minimize the risks involved in the spacecraft sampling operations. The instruments onboard the Rover are a Raman spectrometer (RAX), an infrared radiometer (miniRad), two forward-looking cameras for navigation and science purposes (NavCams), and two cameras observing the interactions of regolith and the rover wheels (WheelCams). The Rover will be deployed before the MMX spacecraft samples Phobos' surface and will be the first rover to drive on the surface of a Martian moon and in a very low gravity environment.

Keywords: Camera, Numerical modelling, Phobos, Radiometer, Raman spectrometer, Regolith, Regolith dynamics, Thermal inertia, Rover

*Correspondence: michelp@oca.eu
†Joint first authors: P. Michel and S. Ulamec contributed equally to this work
[1] Université Côte d'Azur, Observatoire de la Côte d'Azur, CNRS, Laboratoire Lagrange, Nice 06304, France
Full list of author information is available at the end of the article

Graphic Abstract

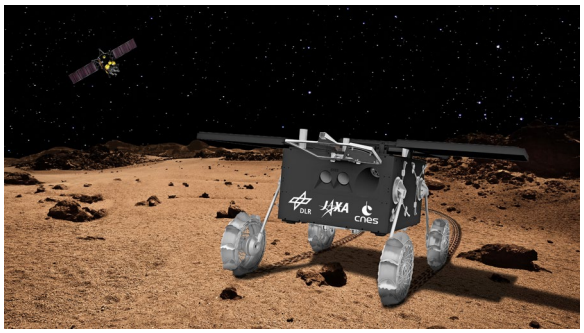

Introduction

The Martian Moons eXploration (MMX) mission by the Japan Aerospace Agency, JAXA, will visit the Martian moons Phobos and Deimos (Kuramoto et al. 2021; Kawakatsu et al. 2019). The MMX Rover, a contribution by the Centre National d'Etudes Spatiales (CNES) and the German Aerospace Center (DLR) to the MMX mission, will be delivered to the surface of Phobos. The MMX Rover will perform in situ science, but will also serve as a scout, preparing for the landing of the main spacecraft. The Rover is planned to be released from the mother spacecraft at an altitude of less than 100 m (the current baseline foresees 45 m), before ballistically descending to the surface of Phobos and coming to rest in an arbitrary attitude after several bounces. The rover will then upright itself and deploy its solar panels. In addition to its scientific objectives, described in the following section, the MMX Rover will demonstrate locomotion on wheels in a very low-gravity environment. The distance that the rover can move on the surface of Phobos will strongly depend on the surface terrain. As the terrain is not yet known, no strict locomotion requirements (such as described in, e.g., Lorenz 2020) have been set. During the rover mission, a total distance from a few metres to hundreds of metres may be covered. The MMX mother spacecraft will act as a relay for all telemetry and commands between the Earth and the rover. More details on the rover system are given by Ulamec et al. (2019).

General science objectives

The scientific objectives of the MMX rover are defined in line with those of the overall MMX mission (Kuramoto et al. 2021), complementing the science which can be performed with the instruments on board the main spacecraft or the returned samples.

These instruments are two navigation cameras (called NavCams), two cameras (called WheelCams) that will observe the interactions of the back and front wheels with the regolith, a Raman spectrometer (called RAX) and a miniaturized radiometer (called miniRad). Figure 1 shows the rover deployed configuration and its internal compartment, while Fig. 2 shows its on-surface configuration.

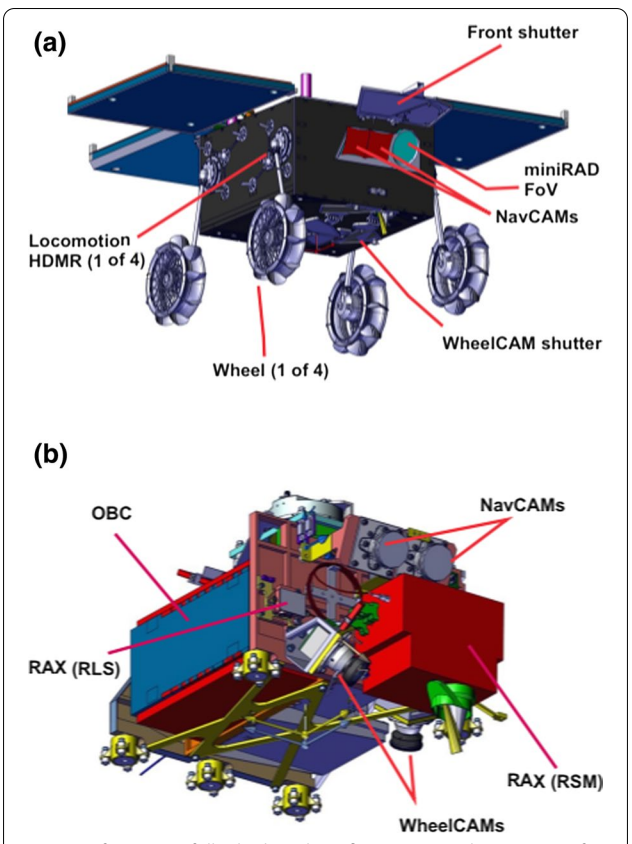

Fig. 1 Left: rover in fully deployed configurations with positions of MiniRad, rear WheelCam and NavCam stereo bench; right: internal compartment (service module—SEM) with position of instruments and on board computer (OBC). Courtesy from CNES

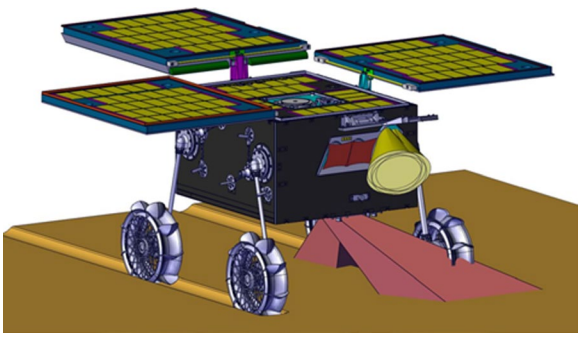

Fig. 2 MMX rover with deployed wheels and solar panels in the on-surface configuration. Field of views of miniRAD and Wheelcams are indicated in yellow and red, respectively. Courtesy from CNES

The data provided by the rover instrument suite are extremely important for the communities interested in regolith dynamics in the low-gravity environment of Phobos, in surface processes, in the formation, geological history and composition of Phobos, and in its thermal properties. The dataset that will be obtained in situ is of high value for the interpretation of data obtained remotely by the MMX spacecraft. It will add ground truth measurements, and provide a geological context to the samples that will be returned to Earth in order to clarify the origin and history of Phobos.

The Rover will perform:

- Close-up and high-resolution imaging of the surface terrain.
- Regolith science (e.g., geometrical properties like grain size and shape distributions; mechanical properties like surface strength; dynamical properties linked to how the regolith flows).
- Measurements of the mineralogical composition of the surface material (by Raman spectroscopy).
- Determination of the thermal properties of the surface material (surface temperature, emissivity, thermal conductivity, layering).

Past images of the surface of Phobos indicating, for example, the very low measured thermal inertia values (a factor 4 lower than that of the asteroid Ryugu, see Table 2) imply that Phobos is covered by a layer of regolith. However, the mechanical properties of Phobos' regolith are poorly constrained. This is mostly due to the difficulty of using remote images to estimate the particle sizes, particle size-distributions, the packing density of the regolith, and other parameters such as friction and cohesion. Note that the highest resolution global imaging of Phobos, performed by the high-resolution stereo camera (HRSC) of Mars Express, is only about 12 m per pixel (Wählisch et al. 2014). The HRSC or the Mars Orbiter Camera (MOC) onboard Mars Global Surveyor have acquired higher resolution images of some limited areas on the surface of Phobos. However, the resolution of these images are still, at best, 1 to 7 m per pixel.

The outcome of the impact experiment performed by the Small Carry-on Impactor (SCI) of the Hayabusa2 mission on the asteroid Ryugu on April 5, 2019 (Arakawa et al. 2020) is a great demonstration that our expectations of the surface response of low-gravity bodies based on remote surface images can be entirely wrong. The crater produced by the SCI was a factor 6-7 larger than predicted by modelling under the expectation that the surface had some cohesion (Arakawa et al. 2020). This is just one example that shows clearly that surface mechanical properties and behaviours in low gravity can be counterintuitive. Therefore, the only way to characterize the regolith properties and response of a low-gravity object and the regolith dynamics is to perform, observe and interpret direct interaction(s) with the surface.

The regolith-covered surface of Phobos preserves records of geophysical processes that have occurred both at the surface and possibly also in the interior. As a result of the low-gravity environment of Phobos, its complex and varied geophysics challenges our understanding. In fact, the field of regolith dynamics in varying gravitational environments has only recently evolved in planetary science. This field will continue to develop thanks to new data from space missions, like those the rover will obtain, as well as the development of better computational tools, experimental techniques and refinements in the theoretical models (Murdoch et al. 2015). To trace back the surface history of Phobos, from its current state back to its formation, which is necessary to test possible formation scenarios, we need to understand how this surface evolved and reacted in response to the different processes during its history.

To do so, a good understanding is needed of the detailed physical properties of the regolith (grain size and shape distribution, friction and cohesive properties, etc.) as well as dynamical properties (how the regolith flows and responds to an external action in the low-gravity environment of Phobos), and compositional and thermal properties. Although regolith analogs for Phobos have been produced (Miyamoto et al. 2021), the assumptions upon which the analogs are based are not necessarily correct. Furthermore, regolith processes on Phobos do not have ready terrestrial analogs, and reduced-gravity experiments are very limited, as they are usually short in duration and very difficult to adjust to the specific gravity conditions of Phobos (about 1/2000 g). The only satisfying way to characterize the physical, microscale compositional and thermal regolith properties of Phobos as well

as the regolith dynamics is to perform in situ measurements of these characteristics, which is precisely what the set of instruments onboard the rover will do (see Table 1 for a summary version of the rover science matrix). These pieces of information control granular material behaviour and are among the most essential parameters for designing and securing the landing and sampling of Phobos' surface material, and also for unique scientific understanding of surface processes taking place on Phobos as well as its surface history.

Although the rover is not equipped with a dedicated instrument for directly probing the subsurface properties (e.g., a ground-penetrating radar or seismometer), the rolling of the rover wheels should generate tracks/trenches exposing the underlying material down to the track/trench depths. This underlying material can be investigated with the rover instruments and, combined with the analysis of the morphologies of the tracks/trenches, will provide unique information on the subsurface structure in the mm to cm range.

In addition to characterizing the physical properties of the surface material on Phobos, the rover will also measure its mineralogical composition by Raman spectroscopy (Cho et al. 2021). Measuring the composition at various spots (possibly even of various individual grains) along the rover path gives ground truth measurements, but also characterizes the heterogeneity of the regolith, providing important context information for the returned samples.

Finally, the measurements by the MMX rover will support the MMX landing and sampling operations. The characterization of the regolith properties shall considerably reduce the risk of the landing (and sampling) of the main MMX spacecraft, as the rover will offer the only direct measurements of Phobos' surface response to an external action prior to these operations.

Science with the Raman spectrometer (RAX)

The top-level science objectives of the MMX mission as defined by JAXA include gaining knowledge about the origin, evolution, and formation of Phobos and Deimos. The determination of the surface composition helps to understand the geochemical, thermal, and radiation processes to which Phobos has been exposed during its existence and that led to the formation of the minerals to be identified and investigated. The occurrence and co-occurrence of mineral phases like hydrated phyllosilicates and carbonates are directly pointing to the "Capture of organic- and water-rich outer solar system body" origin hypothesis for Phobos. In contrast, the existence of evolved, basaltic mineralogy consistent with many datasets from Mars would support the "Giant impact on Mars" origin hypothesis. The Raman spectrometer onboard the rover will be used to provide in situ information about Phobos' mineralogical composition at the micrometre scale.

The Raman spectrometer for MMX (RAX) (Fig. 3) is a compact, low-mass instrument with a volume of approximately $81 \times 98 \times 125$ mm^3 and a mass of less than 1.4 kg. RAX was developed by DLR, INTA/UVA and JAXA/UTOPS/Rikkyo (for more information see Cho et al. (2021), this issue). It is designed to withstand the harsh conditions on Phobos and will be the first Raman spectrometer on an airless body. The measurements performed with RAX include the identification of minerals on various points on the surface of Phobos, validated by comparison with experiments in laboratories on Earth and with spectral laboratory reference databases. The acquired data will support and complement the orbiter spectroscopic measurements, and will provide ground truth measurements performed on the returned samples. Furthermore, the RAX data will be compared with the results obtained with the Raman spectrometer RLS during the ExoMars2022 mission on the surface of Mars. The combination of the in situ, remote and Earth laboratory based measurements brings us a big step forward to better understand the origin of its moons.

Science with the miniaturized radiometer (miniRAD)

The miniaturized radiometer (miniRAD) will investigate the surface temperature of Phobos by measuring the radiative flux emitted in the thermal infrared wavelength range using thermopile sensors (Kessler et al. 2005). The instrument, which will be mounted in the front compartment of the rover, has strong heritage from the Rosetta MUPUS thermal mapper (Spohn et al.

Fig. 3 CAD model of RAX

2007), the MASCOT radiometer (Grott et al. 2017), and the InSight radiometer (Spohn et al. 2018; Müller et al. 2020). The six miniRAD sensors have a field of view of 45° and will observe a spot at a distance of ∼25 to ∼150 cm in front of the rover, which will be located within the field of view of the stereo navigation cameras (NavCams, see below). In this way, geological context for the miniRAD observations will be provided along with a digital terrain model of the scene.

The surface temperatures T on Phobos are governed by the surface energy balance, which is driven by insolation S and given by

$$\sigma_B \varepsilon T^4 = (1-A)S + \Gamma \sqrt{\frac{\pi}{P}} \left. \frac{\partial T}{\partial z'} \right|_{z'=0}, \quad (1)$$

where σ_B is the Stefan–Boltzmann constant, ε is surface emissivity, A is bond albedo, P is Phobos' rotation period, and $z' = z/d$ is depth z normalized to the skin depth $d = \sqrt{kP/\rho c_p \pi}$. Here, ρ is the material's bulk density, c_p is heat capacity, and k is thermal conductivity. In Eq. 1, the thermal inertia

$$\Gamma = \sqrt{k \rho c_p} \quad (2)$$

is the material parameter governing the surface's temperature response to heating, where low values of Γ correspond to fast changes and vice versa. Therefore, given surface emissivity as well as surface temperature, the material's thermophysical parameters can be estimated (Hamm et al. 2018).

Previously determined thermal inertia values for Phobos are summarized in Table 2. The values are generally found to be quite low, in the 20 to 85 J m^{-2} K^{-1} s$^{-1/2}$ range. Fig. 4 shows the derived thermal conductivity as a function of temperature for Phobos as well as for C-class asteroids, S-class asteroids, average near-Earth asteroids, and comets. The thermal conductivity of the lunar regolith is also shown as a reference. Current best estimates of thermal conductivity for Phobos are similar to the lunar value, and this has generally been interpreted in terms of a surface covered with fine-grained regolith with average particle diameters in the few millimeter range (Gundlach and Blum 2013). Furthermore, the reported low thermal conductivity indicates a low surface rock abundance, likely in the few percent range.

The interpretation of the available thermal infrared data for Phobos is complicated by the fact that to date, all available datasets cover only a limited range of local times. However, the influence of, e.g., surface roughness (Kuehrt et al. 1992) or layering is best studied considering the entire diurnal temperature curve. Surface roughness strongly affects thermal emission on airless bodies (Kuehrt et al. 1992; Davidsson et al. 2015). Its effect on emitted flux is shown in Fig. 5, where the ratio of the flux emitted by a rough surface to that emitted

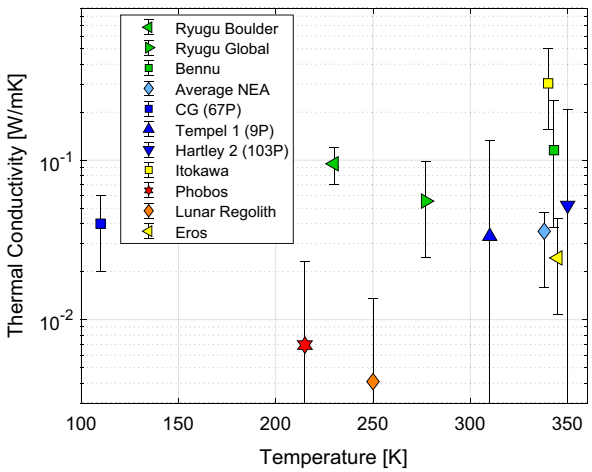

Fig. 4 Thermal conductivity as a function of temperature as derived for different small bodies. Data for C-class asteroids Bennu (Emery et al. 2014; Dellagiustina et al. 2019; Rozitis et al. 2019) and Ryugu (Müller et al. 2017; Hamm et al. 2020), for average near-Earth asteroids (Delbo et al. 2007), for comets 9P/Tempel 1 (Groussin et al. 2013; Davidsson et al. 2009), 103P/Hartley (Groussin et al. 2013), and 67P/Churyumov–Gerasimenko (Spohn et al. 2015), for S-class asteroids Itokawa (Fujiwara et al. 2006) and Eros (Lebofsky and Rieke 1979; Harris and Davies 1999) are shown together with the current best estimate for Phobos (Kuzmin and Zabalueva 2003). For comparison, the thermal conductivity of the lunar regolith (Hayne et al. 2017) is also given

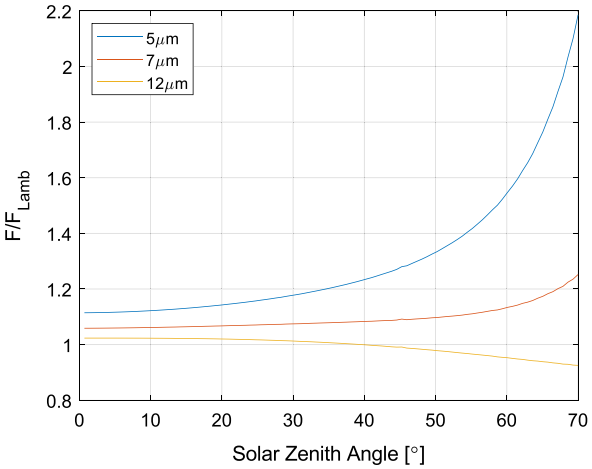

Fig. 5 The ratio of flux emitted by a rough surface to that emitted by a flat Lambertian surface as a function of solar zenith angle at three different wavelengths. Results are shown for an equatorial location and a south facing instrument, which observes the surface under an emission angle of 45°

by a flat Lambertian surface is shown as a function of solar zenith angle. The employed roughness model (Giese and Kuehrt 1990; Kuehrt et al. 1992; Lagerros 1996) considers a surface covered by hemispherical craters, a crater density of 50%, a bond albedo of 0.02, an emissivity of 0.95, and a heliocentric distance of 2 AU. As is evident from the figure, roughness can dramatically change the flux received by the instrument when compared to a flat surface, and this effect is most pronounced at short wavelengths under low sun conditions. Therefore, observing temperatures for a full day–night cycle over the entire range of solar incidence angles provides data that can help to resolve some of the inherent ambiguities when interpreting received flux in terms of surface temperatures. Furthermore, measurements at different wavelengths can help to disentangle surface roughness from thermal inertia.

The sensing depth of thermal infrared observations is of the order of a few diurnal skin depths d. The latter is expected to be close to 5 mm for Phobos' regolith and of the order of a few centimetres for typical boulders. Therefore, shallow regolith layering or the presence of a thin veneer of low thermal inertia dust covering bedrock or boulders should be detectable by thermal infrared measurements. Layering has a pronounced effect on surface temperatures (Biele et al. 2019; Grott et al. 2019), and cooling rates after sunset are particularly sensitive. Therefore, data covering full diurnal temperature cycles can be used to constrain the presence or absence of layering, as has been done for a boulder on asteroid Ryugu during its visit by the JAXA Hayabusa2 spacecraft using the lander MASCOT radiometer data (Grott et al. 2019).

The miniRAD instrument onboard the MMX rover will observe the surface of Phobos in 6 distinct wavelength bands and investigate different geological units along the rover's traverse. Surface temperatures of fine-grained regolith as well as boulders will be determined for full diurnal cycles, thus enabling interpretation of the data in terms of thermophysical properties, roughness, and layering. For granular materials, miniRAD will determine the regolith thermal conductivity, porosity, and particle size (Ogawa et al. 2019), while for boulders, the thermal conductivity as well as the porosity can be determined. The miniRAD data will be diagnostic for determining the potential presence of thin dust coverings on boulders, and the influence of surface roughness will be quantified by observing the same target in different wavelength bands. In this way, material properties can be determined and directly compared to those of other small bodies and known meteorites (e.g., Flynn et al. 2018), shedding light on the moon's formation and evolutionary processes.

Science with the navigation cameras (NavCams)

The NavCams are a set of stereo cameras (two cameras, aligned on a bench) observing the landscape in front of the rover (Fig. 6). As their name indicates, their purpose is to allow both for the navigation of the rover and its progression (autonomously or commanded from ground) on the possibly rough terrain of Phobos. The NavCams will also perform unprecedented science at the surface of Phobos.

The cameras are based on a microcamera cube CMV-4000 developed by CNES and 3DPLUS company. The image sensor consists of a 2048 by 2048 array (4 Mpixel), with each pixel having a 5.5μm pitch. It is based on a

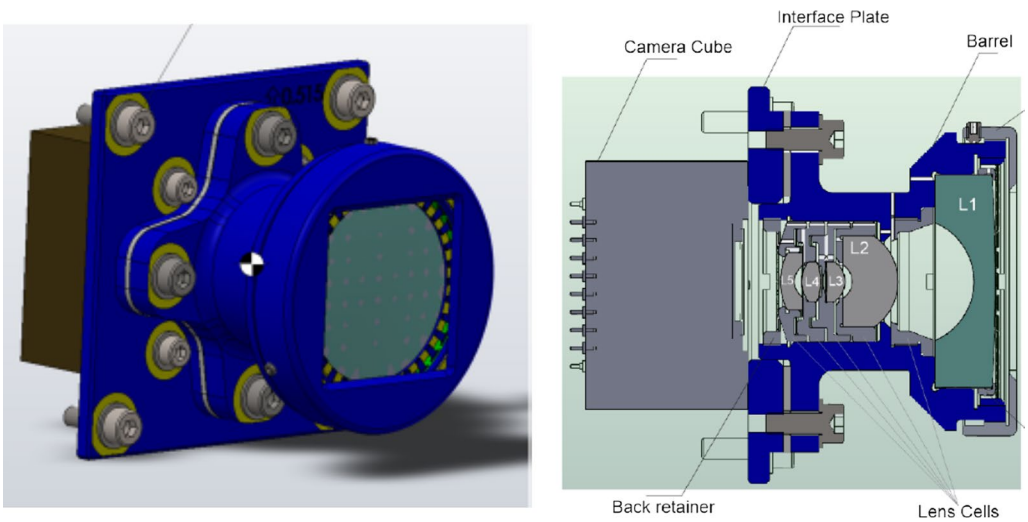

Fig. 6 The navigation cameras (NavCams). Left: CAD view; right: schematic view

pinned photodiode to minimize the noise and achieve high electro-optic performances. For the NavCams, this microcamera cube is equipped with a colour image sensor (Bayer filter, i.e. forming a RGGB 2×2 mosaic that repeats across the detector). The optics lead to a field-of-view of 118° in diagonal and 83° edge-to-edge. The resulting field depth allows images of the surface to be acquired from 35 cm up to infinity. At a distance of 1 m, the spatial resolution is about ~1 mm per pixel.

Beyond the identification of areas of interests, the NavCam images will allow the surface topography and morphologies to be characterized at high spatial resolution. The NavCam images will also allow the spatial distribution of the blue and red materials, already detected at a lower spatial resolution on Phobos (e.g., Thomas et al. 2011; Pieters et al. 2014), to be determined. Indeed, Phobos exhibits a heterogeneous surface with two spatially coherent units, one with a spectrum that is modestly red (commonly called the blue unit) and the other with a spectrum that slopes more steeply into the near-infrared (commonly called the red unit) (Pieters et al. 2014). The blue unit is essentially found within and around the large crater Stickney and a generic relation with the crater has often been presumed.

To fulfil the NavCam scientific objectives, we will generate 1) geo-referenced digital terrain models (DTMs), 2) albedo maps, and 3) low-resolution spectral maps.

Both the albedo and the low-resolution spectral maps will allow progress to be made in our understanding of the origin of the blue and red materials. Indeed, both materials possess distinct spectral slopes and albedos in the visible range with blue materials being substantially brighter than red materials (e.g., Thomas et al. 2011; Pieters et al. 2014). As of today, no simple spatial distribution nor stratigraphic relation between these materials can be discerned (Pieters et al. 2014). There is also no apparent colour–age relation for small craters: fresh (recent) craters expose either type of material at different locations (Pieters et al. 2014). Given the observed spatial relationships, it is currently difficult to formulate a single model through which the red unit is largely a depositional unit or is derived from the blue unit by some form of space weathering.

The local high-resolution DTMs will be geo-referenced to the global DTM of Phobos reconstructed from the orbiter camera (TENGOO). The unprecedented resolution of the local DTMs will allow us to identify and characterize small-scale topographic features such as grains, boulders and cracks. These DTMs will allow the size distribution of the grains to be constrained down to ~1 mm and may allow monitoring of any regolith movement and/or albedo variation on short timescales. The local DTMs will be a key complement to the geomorphologic analyses performed with the orbiter camera observations for the whole surface and will allow us to refine our understanding of the overall geological history of Phobos.

Science with the wheel cameras (WheelCams)

The WheelCams are a set of two cameras placed on the underside of the rover and each aimed at a different wheel (Fig. 7). Their primary purpose is to observe the wheels and the behaviour of the regolith around the wheels as the rover is advancing, providing unique information on the mechanical properties and dynamics of the regolith in the low-gravity environment of Phobos. Their secondary purpose is to provide multispectral images at very high resolution of the Phobos soil using coloured LEDs.

The cameras are based on the same microcamera cube as the NavCams (see previous section). However, the detector is panchromatic (no colour filter). The

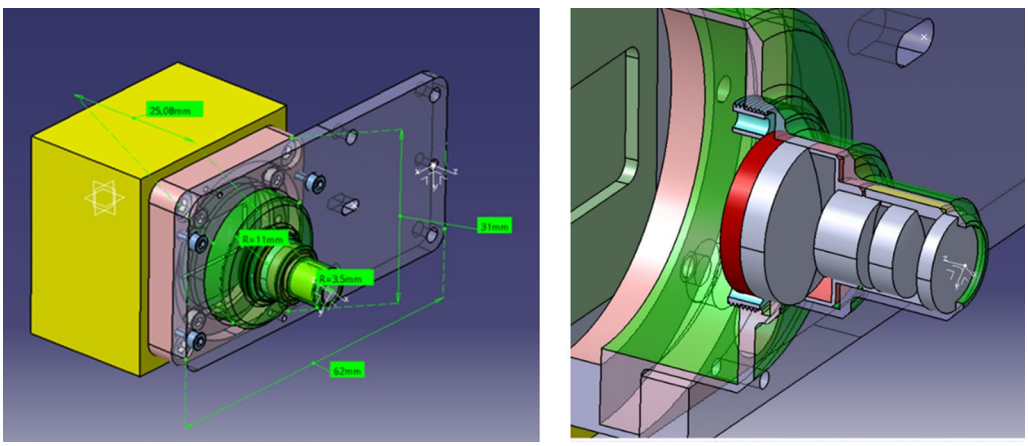

Fig. 7 The wheel cameras (WheelCams) in their pre-phase A design. Left: CAD view; right: schematic view

optics provide a field of view of 32.5°, a best focus distance of 35 cm, and a field depth of 10 cm. This gives a pixel resolution of approximately 100 μm at the centre of the image.

In order to illuminate the scene, which is almost always in the shadow of the rover body and solar panels, they are equipped with LEDs. Some are "high power" (0.5 W) white LEDs to be used while driving, while others are colour LEDs of specific bandwidths to allow for multispectral imaging. These colour LEDs are the Epitex L590-09, the USHIO L720-2AU and the EOLD-880-525 at, respectively, 590 nm, 720 nm and 880 nm (Boutillier et al. 2014).

The WheelCams can be used with the white LED while the rover is driving (the typical image frequency will be about one picture every second for a motion of about 1 mm/s), or at night with the colour LEDs and with longer exposure times. Due to the huge data volumes produced by the image sequences, they are binned down to 1024 by 1024 images and cropped to retain only the most important part of the picture. Temporal compression of the image sequences is also considered, but not confirmed at this stage. On the other hand, the detailed night images with the colour LEDs are transmitted with lossless compression (no binning or cropping).

The physical properties of Phobos' surface are closely linked to the history and origin of the body. Such information also has important implications for spacecraft–surface interactions such as the landing of the main MMX spacecraft and the surface sampling. Given that remote observations can often lead to very different interpretations on surface and internal properties, the only way to truly probe the mechanical and physical properties is to directly interact with the surface material. By observing the surface and the interactions between the rover wheels and the regolith, the WheelCams will study the mechanical and dynamical properties of Phobos' regolith.

The WheelCams will be used to characterize the general grain properties of Phobos' regolith. Specifically, the high-resolution WheelCam images will allow the regolith particles to be identified down to particle sizes of approximately 200 μm. Combining this information with local high-resolution DTMs from the NavCams, and images and global DTMs from the main MMX spacecraft will provide the particle size distribution, spanning many more orders of magnitude than previous studies of Phobos (Thomas et al. 2000). The slope of the particle size distribution can indicate how much processing (impacting, breaking, size sorting, transporting) Phobos' regolith has experienced. The grain morphologies (sphericity and angularity) will also be investigated (for grains > 1 mm) using the WheelCam images.

The rover wheel–regolith interactions will also be investigated in detail; the WheelCams will determine the depth of the wheel sinkage, which is closely linked to the load bearing strength and friction angle of the regolith (Sullivan et al. 2011). Observations of talus in the rover tracks and tailings behind the wheels provide measurements of the angle of repose, and undisturbed trench walls provide a lower limit to the regolith cohesion (Sullivan et al. 2011). In addition, measurement of traction and slippage (e.g., Maimone et al. 2007; Reina et al. 2006) will provide shearing characteristics of the regolith. These numerous WheelCam observations will be compiled in order to characterize the bulk properties of the regolith. The observations will also improve our understanding of granular flow on Phobos and in reduced-gravity environments in general, with profound implications on Phobos' surface history.

Numerical modelling for supporting rover dynamics and interpreting regolith properties

The instruments onboard the MMX rover will provide substantial information on the small-scale topographic features and grain properties of Phobos' surface. The mechanical and dynamical behaviour of regolith materials both in the quasi-static and flowing regimes will be intensively characterized by the WheelCams. However, the MMX rover will be the first wheeled rover in a milligravity environment. Therefore, the established knowledge about rover dynamics and regolith behaviour from Lunar and Martian exploration and from Earth laboratory experiments is not necessarily applicable to Phobos. Recent small-body missions (i.e. Hayabusa2 and OSIRIS-REx) have shown that the responses of these airless, low-gravity small-body surfaces to robotic maneuvers are significantly different from those observed in an Earth-gravity environment (Arakawa et al. 2020; Lauretta et al. 2021).

As an effective test bed for various physical properties and dynamical processes, numerical modelling is crucial to the design of the locomotion system (Sedlmayr et al. 2020) and potentially other platform systems. Simulations are also required to help with the interpretations of the WheelCam images in order to determine the mechanical properties of the regolith. Validated material models and parameters can be further used to simulate the geophysical evolution of Phobos over its lifetime. Combined with the regolith mineralogical composition and thermal properties measured by the RAX and miniRad instruments, respectively, numerical modelling will help to constrain the origin and evolution of Phobos.

To fulfil the above science objectives, at least two complementary numerical approaches, with discrete and continuum treatments, respectively, will be used to study

the rover and regolith dynamics in the actual low-gravity environment of Phobos. Continuum numerical modelling of granular material usually begins by defining a systematic approach to averaging the physics across many particles (and thereby treating the granular material as a continuum). However, the homogenization of the granular-scale physics is not necessarily appropriate, and the discreteness of the particles and the forces between particles need to be taken into account. The discrete element method (DEM) is a general term applied to the class of discrete approaches to the numerical simulation of particle motion, where particles usually represent actual grains (or collections of grains), and the simulations solve all contact forces between them. Both the continuum and the discrete approach can be useful to model the regolith response to the rolling motion of the rover. Ideally, the best approach is the one that models each grain and its behaviour directly. This is the goal for DEM simulations, however, it is sometimes impossible to do so because of high computational costs. In particular, for a regolith made of a dense collection of extremely fine grains, the continuum approach may be best suited and more efficient, while for a regolith made of a dilute collection of coarse grains, the discrete approach can certainly be adopted. In the following, we briefly present the two approaches and how we plan to apply them to the MMX rover.

Soft-sphere discrete element method (SSDEM)

The soft-sphere discrete element method (SSDEM) is a highly accurate but costly option for studying rover interactions with granular surfaces. In this method, the overall behaviour of the system is determined by calculating the contact forces acting on each grain in a regolith bed and then advancing the system accordingly. Contacts are evaluated at small time intervals, where the size of the time-step is dependent on the properties of the grains. In general, stiffer surface materials will result in smaller time-steps and longer processing times. A key benefit of SSDEM is that this method effectively captures the influence of gravity and cohesion on granular flows without relying on empirical or semi-empirical relationships. SSDEM has proven to be an effective tool for advancing research related to the formation and evolution of small bodies (Sanchez and Scheeres 2014; Zhang and Lin 2020; Michel et al. 2020). This method has also been used to assess the performance of planetary rovers, though most commonly for the gravity environments found on the moon and Mars (Nakashima et al. 2007; Johnson et al. 2015). Currently, DLR is using DEM to assist with the design and optimization of the MMX rover wheel for Phobos-like surface conditions (Buchele and Lichtenheldt 2020).

A significant challenge associated with DEM is selecting the appropriate simulation parameters when the material properties of the surface are largely unknown. For the rover studies, simulations can be conducted for the entire range of soil cases presented in the previous sections. Then, the results can be used to create a map between observable outcomes like trench shape, wheel sinkage, and wheel slip, and important material properties like those discussed in the section presenting the science of the WheelCams, such as cohesion and internal friction.

Fig. 8 provides an example of a typical simulation with a simplified rover wheel and a bed of large, spherical particles. In addition to wheel sinkage, the grain-scale resolution of DEM allows us to observe the shear-band created by the granular flow under the wheel.

Continuum method

A continuum description of dense granular materials can be used as a fast and coarse approach to model the rheology of granular beds. In this type of description, local particle velocities are averaged, resulting in a continuous velocity field (Da Cruz et al. 2005). Additionally, forces between particles are averaged up to viscous stress and pressure fields, similar to the Navier–Stokes equation for viscous fluids.

A first version of a continuous model for dense granular flows was proposed by Jop et al. (2006), based on the expression of an apparent (in the macroscopic sense) friction coefficient μ. This model makes it possible to reproduce the viscoplastic effects and the dependence on normal stresses observed experimentally and numerically using discrete numerical simulations (Da Cruz et al. 2005), such as the existence of a flow threshold, the

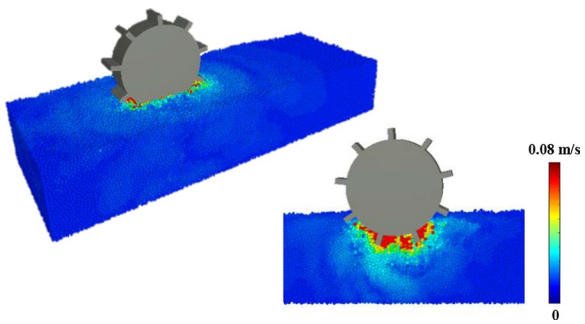

Fig. 8 Example of a SSDEM simulation of a simplified MMX rover wheel traversing a bed of 180,000 cohesionless spherical grains. The wheel is 214 mm in diameter and the grains are 6 ± 0.5 mm in diameter. The simulation was conducted under Earth-gravity using Chrono (Sunday et al. 2020). The grains are coloured by velocity magnitude

Table 1 Summary version of the rover science traceability matrix

MMX Science goal	Science objective	Measurement objective	Technique	Instrument
Origin of the body	Determine the surface composition and formation conditions	Identification of mineralogical composition at grains scales, igneous phase and secondary alteration	Reflectance, albedo and spectral slope measurements	Wheelcams with LED illumination
			Color-fine scale imagery	NavCams
			Camera imaging of regolith	RAX with LED illumination
			Spectroscopy	RAX - Raman spectroscopy
				RAX - NIR (535 nm - 680 nm) Spectroscopy with LED illumination
		Organic and volatile species identification	Raman spectroscopy	RAX - Raman spectroscopy
		Determine the location of the Christiansen Feature	Radiometric surface brightness determination at wavelengths of 8.2, 8.9, and 9.4 µm	miniRAD
		Determine the spectral slope in the IR wavelength range	Radiometric surface brightness determination at wavelengths of 4.7, 8.2, 8.9, and 9.4 µm	miniRAD
		Determine surface roughness	Radiometric surface brightness determination at 4.7 µm	miniRAD
		Determine dust cover thickness / layering	Radiometric surface brightness determination in the broadband channels	miniRAD
		Determine diurnal temperature amplitude / thermal fatigue	Radiometric surface brightness determination in the broadband channels	miniRAD
	Determine the origin of the blue and red materials	Spatial distribution and stratigraphic relation between the blue and red materials	Reflectance, albedo and spectral slope measurements	Wheelcams with LED illumination
			Color-fine scale imagery	NavCams
			Raman spectrsocopy	RAX - Raman spectroscopy
	Determine the internal structure/sub-surface. Constrain the global physical properties	Absolute local gravitational acceleration	Balistic tracking of particles ejected during locomotion	WheelCams
		Mechanical properties of the surface material	Camera imaging of regolith, wheel-regolith interactions and trenches	WheelCams
			Camera imaging of natural features, Camera imaging of trenches*	NavCams
	Correlate mineral/rock types and abundancies of Phobos and Mars	Comparison with measurements on Mars (RLS-ExoMars)	Raman spectroscopy	RAX - Raman spectroscopy
	Correlate the mineralogy derived from measurements on Phobos with that derived from returned samples	Contribution to sample return and to science on returned samples	Raman spectroscopy	RAX - Raman spectroscopy

Table 1 (continued)

Surface evolution and processes	Characterisation of physical properties and dynamics of regolith	Grain & boulder size distribution	> 0.2 mm	Camera imaging of regolith	WheelCams
			> 1 mm	Camera imaging of regolith	NavCams
			>10 µm, < 2 mm	Camera imaging of regolith	RAX with slant LED illumination for shadow analysis
		Grain & boulder shape (sphericity/angularity)	> 1 mm	Camera imaging of regolith	WheelCams
			> 5 mm	Camera imaging of regolith	NavCams
		Determination of regolith geological classes (e.g., drift/loose soil, crusty/cloddy, blocky, ...)		Camera imaging of regolith, wheel-regolith interactions and trenches	WheelCams
				Camera imaging of regolith	NavCams
		Layering in the very shallow sub-surface		Camera imaging of trenches	WheelCams
				Camera imaging of natural features, Camera imaging of trenches*	NavCams
		Angle of friction (inferred)		Camera imaging of wheel-regolith interactions and trenches	WheelCams
				Camera imaging of natural features, Camera imaging of trenches*	NavCams
		Cohesion (inferred)		Camera imaging of wheel-regolith interactions and trenches	WheelCams
		Adhesion of the regolith to the rover		Camera imaging of wheels	WheelCams
		Determine surface thermal inertia		Measure surface brightness temperature in the broad-band channels	miniRAD
		Determine thermal conductivity		Measure surface brightness temperature in the broad-band channels	miniRAD
		Determine porosity		Measure surface brightness temperature in the broad-band channels	miniRAD
	Surface alteration	Quantify the space weathering		Imaging inside the trenches, compared with on the surface	Wheelcams with LED illumination
				Color-fine scale imagery inside the trenches, compared with on the surface*, Stratigraphy on large boulders	NavCams
	Characterisation of Phobos' grooves	Groove occurrence and distribution at small scale		Camera imaging and Digital Terrain Model (DTM)	NavCams
	* This would involve the rover turning around. This will be very slow and will not be done systematically.				

Table 2 Estimates of Phobos' thermal inertia

Mission	Thermal inertia [J $m^{-2} K^{-1} s^{-1/2}$]	Remarks	References
Viking	25–85		Lunine et al. (1982)
Phobos 2	33–83		Ksanfomality et al. (1989)
Phobos 2	20–40	Incl. surface roughness	Kuehrt et al. (1992)
MGS	70	First spatially resolved measurements	Smith et al. (2018)
Mars Odyssey	50	Indication of layering	Bandfield et al. (2018)

dependence of μ on speed, pressure, size and density of grains. In this model, the apparent friction is an increasing function of a single parameter I, called an inertial number, defined by $I = \dot{\gamma} d/(P/\rho)^{0.5}$, where $\dot{\gamma}$, d, P and ρ are, respectively, the second invariant of the strain rate tensor, the mean particle diameter, the confining (macroscopic) pressure and the grain density. This parameter measures the relative contribution of the inertial (or kinetic) pressure to the confining (static) pressure.

This so-called $\mu(I)$ model has been successfully applied to predict rheometric shear flows, stationary one- and two-dimensional free surface flows (GDR MiDi group 2004) as well as three-dimensional transient free surface flows (Valette et al. 2019), using numerical simulations.

Recent extensions of the $\mu(I)$ model, such as the one proposed by Vo et al. (2020), make it possible to take into account both cohesive and viscous effects in the same formalism. In this continuous model, the number of parameters is restricted, and will allow multiple conditions for rover interactions with the granular bed to be explored rapidly. Subsequent inverse mapping of continuum to SSDEM models parameters can then accelerate the fine interpretation of WheelCam images using SSDEM.

Conclusions and outlook

The MMX mission will provide the first detailed information on Phobos, and the first sample of a Martian moon for analysis in laboratories on Earth. The rover that the spacecraft will deploy on Phobos' surface will obtain the first in situ information on the compositional and physical properties of the surface of this moon, as well as on the mechanics and dynamics of regolith in the corresponding gravitational environment. Direct measurements of the surface response to an external action, such as the rolling of rover's wheels, are of unique value both for scientific and technical purposes. Comparison between the microscale properties measured by the rover and macroscale ones measured by the instruments onboard the main MMX spacecraft, as well as the sample analyses, will be of high value. These combined measurements will allow the maximum science return of the MMX mission to be achieved.

After having finished Phase B in 2020, the MMX rover development will follow a proto-flight model approach, including a full qualification program. The flight model will be delivered to Japan in 2023, to be integrated to the main MMX spacecraft where a combined testing program is foreseen. The MMX mission is planned to be launched in 2024. After arrival at Phobos in 2025, remote investigations will start, which will include landing and sampling site selections (Nakamura et al. 2021). The rover is currently planned to be delivered to the surface of Phobos in early 2027 and is expected to operate on Phobos for at least 100 days. Telemetry and commands will be relayed via the main MMX spacecraft. There are dedicated Rover Operations centres at DLR in Cologne/Germany and at CNES in Toulouse/France. MMX will leave Mars orbit in 2028 and return to Earth in August 2029 (Kawakatsu et al. 2019) with Phobos samples.

Acknowledgements

The rover on the MMX mission of JAXA is a CNES-DLR cooperation. The authors would like to thank the whole MMX team at JAXA/ISAS for the unique opportunity to participate to this exciting mission.

Authors' contributions

The authors wish it to be known that, in their opinion, the first two authors (PM and SU) should be regarded as joint first authors. All authors read and approved the final manuscript.

Funding

This work benefits from funding by CNES and DLR. CS acknowledges PhD thesis funding from ISAE-SUPAERO and CNES. YZ acknowledges funding from the Université Côte d'Azur "Individual grants for young researchers" program of IDEX JEDI.

Availability of data and materials

Not applicable.

Declarations

Competing interests

The authors declare that they have no competing interests.

Author details

[1]Université Côte d'Azur, Observatoire de la Côte d'Azur, CNRS, Laboratoire Lagrange, Nice 06304, France. [2]Deutsches Zentrum für Luft- und Raumfahrt e.V. (DLR), Space Operations and Astronaut Training, Linder Höhe, 51147 Cologne, Germany. [3]Deutsches Zentrum für Luft- und Raumfahrt e.V. (DLR), Institute of Optical Sensor Systems, Rutherfordstr. 2, 12489 Berlin, Germany. [4]Deutsches Zentrum für Luft- und Raumfahrt e.V. (DLR), Institute of Planetary Research, Rutherfordstrasse 2, 12489 Berlin, Germany. [5]ISAE-SUPAERO, Université de Toulouse, DEOS/Space Systems for Planetary

Applications, 10 avenue Edouard Belin, BP 54032, 31055 Toulouse Cedex 4, France. [6]Aix Marseille Université, CNRS, CNES, Laboratoire d'Astrophysique de Marseille, Marseille, France. [7]Université de Toulouse, DEOS/Space Systems for Planetary Applications, 10 avenue Edouard Belin, BP 54032, 31055 Toulouse Cedex 4, France. [8]Mines ParisTech, PSL Research University, CEMEF, Centre for Material Forming, CNRS UMR 7635, CS 10207 rue Claude Daunesse, 06904 Sophia Antipolis Cedex, France. [9]CNES, BPI 2532, Laplace 116B, 18 avenue Édouard Belin, 31401 Toulouse Cedex 9, France. [10]Deutsches Zentrum für Luft- und Raumfahrt e. V. (DLR), Institute of Space Systems, Robert-Hooke-Strasse 7, 28359 Bremen, Germany. [11]Directorate for Orbital Systems / Science Project Department, 18 avenue Edouard Belin, 31401 Toulouse Cedex 9, France. [12]Deutsches Zentrum für Luft- und Raumfahrt e.V. (DLR), 82234 Oberpfaffenhofen, Germany. [13]Department of Systems Innovation, University of Tokyo, 7-3-1 Hongo, Bunkyo-ku, Tokyo 113-8656, Japan. [14]Laboratory for Early Solar System Evolution, Department of Earth Science, Graduate School of Science, Tohoku University, Aoba, Sendai, Miyagi 980-8578, Japan. [15]Planetary Exploration Research Center (PERC), Chiba Institute of Technology (Chitech), Tsudanuma 2-17-1, Narashino, Chiba 275-0016, Japan. [16]Research and Development Directorate, Japan Aerospace Exploration Agency, Sagamihara 252-5210, Japan. [17]Faculty of Science, Hokkaido University, Kita-10 Nishi-8, Kita-ku, Sapporo 060-0810, Japan.

Received: 1 January 2021 Accepted: 18 June 2021
Published online: 03 January 2022

References

Arakawa M, Saiki T, Wada K, Ogawa K, Kadono T, Shirai K et al (2020) An artificial impact on the asteroid (162173) Ryugu formed a crater in the gravity-dominated regime. Science 368:67–71

Bandfield JL, et al. (2018) Mars Odyssey THEMIS observations of phobos: new spectral and thermophysical measurements. Paper presented at the 49th lunar and planetary science conference 2018, (LPI Contrib. No. 2083)

Biele J et al (2019) Effects of dust layers on thermal emission from airless bodies. Prog Earth Planet Sci 6:48. https://doi.org/10.1186/s40645-019-0291-0

Boutillier M, Gilard O, Quadri G, Lhuillier S, How LS, Hernandez S (2014) Commercial light emitting diodes sensitivity to protons radiations. Paper presented in 2014 IEEE radiation effects data workshop (REDW), Paris, 14-18 July 2014

Buchele F, Lichtenheldt R (2020) Multi-parameter rover wheel and grouser optimization for deployment in Phobos' milli-g environment. In: iSAIRAS 2020: international symposium on artificial intelligence, robotics and automation in space. iSAIRAS 2020, 19–23 Oct 2020, virtual online

Cho Y, Böttger U, Rull F, Hübers H-W, The RAX Team (2021) In-situ science on Phobos with the Raman spectrometer for MMX (RAX): preliminary design and feasibility of Raman measurements. Earth Planets Space. https://doi.org/10.1186/s40623-021-01496-z

Da Cruz F, Emam S, Prochnow M, Roux JN, Chevoir F (2005) Rheophysics of dense granular materials: discrete simulation of plane shear flows. Phys Rev E 72:021309

Davidsson BJR, Gutiérrez PJ, Rickman H (2009) Physical properties of morphological units on Comet 9P/Tempel 1 derived from near-IR Deep Impact spectra. Icarus 201(1):335–357. https://doi.org/10.1016/j.icarus.2008.12.039

Davidsson BJR, Rickman H, Bandfield JL, Groussin O, Gutiérrez PJ, Wilska M, Capria MT, Emery JP, Helbert J, Jorda L, Maturilli A, Mueller TG (2015) Interpretation of thermal emission. I. The effect of roughness for spatially resolved atmosphereless bodies. Icarus 252:1–21. https://doi.org/10.1016/j.icarus.2014.12.029

Delbo' M, dell'Oro A, Harris AW, Mottola S, Mueller M (2007) Thermal inertia of near-Earth asteroids and implications for the magnitude of the Yarkovsky effect. Icarus 190:236–249. https://doi.org/10.1016/j.icarus.2007.03.00

Dellagiustina DN et al (2019) Properties of rubble-pile asteroid (101955) Bennu from OSIRIS-REx imaging and thermal analysis. Nat Astron 3:341–351. https://doi.org/10.1038/s41550-019-0731-1

Emery JP et al (2014) Thermal infrared observations and thermophysical characterization of OSIRIS-REx target asteroid (101955) Bennu. Icarus 234:17–35. https://doi.org/10.1016/j.icarus.2014.02.005

Flynn GJ, Consolmagno GJ, Brown P, Macke RJ (2018) Physical properties of the stone meteorites: implications for the properties of their parent bodies. Chemie der Erde Geochem 78:269–298. https://doi.org/10.1016/j.chemer.2017.04.002

Fujiwara A et al (2006) The rubble-pile asteroid itokawa as observed by Hayabusa. Science 312:1330–1334. https://doi.org/10.1126/science.1125841

GDR MiDi group (2004) On dense granular flows. Eur Phys J E 14:341–365

Giese B, Kuehrt E (1990) Theoretical interpretation of infrared measurements at Deimos in the framework of crater radiation. Icarus 88:372–379. https://doi.org/10.1016/0019-1035(90)90088-Q

Grott M et al (2017) The MASCOT radiometer MARA for the Hayabusa 2 mission. Space Sci Rev 208:413–431. https://doi.org/10.1007/s11214-016-0272-1

Grott M et al (2019) Low thermal conductivity boulder with high porosity identified on C-type asteroid (162173) Ryugu. Nat Astron 3:971–976. https://doi.org/10.1038/s41550-019-0832-x

Groussin O et al (2013) The temperature, thermal inertia, roughness and colour of the nuclei of Comets 103P/Hartley 2 and 9P/Tempel 1. Icarus 222:580–594. https://doi.org/10.1016/j.icarus.2012.10.003

Gundlach B, Blum J (2013) A new method to determine the grain size of planetary regolith. Icarus 223:479–492. https://doi.org/10.1016/j.icarus.2012.11.039

Hamm M, Pelivan I, Grott M, de Wiljes J (2020) Thermophysical modelling and parameter estimation of small Solar system bodies via data assimilation. Mon Note R Astron Soc 496:2776–2785. https://doi.org/10.1093/mnras/staa1755

Hamm M, Grott M, Kuehrt E, Pelivan I, Knollenberg J (2018) A method to derive surface thermophysical properties of asteroid (162173) Ryugu (1999JU3) from in-situ surface brightness temperature measurements. Planet Space Sci 159:1–10. https://doi.org/10.1016/j.pss.2018.03.017

Harris AW, Davies JK (1999) Physical Characteristics of Near-Earth Asteroids from Thermal Infrared Spectrophotometry. Icarus 142:464–475. https://doi.org/10.1006/icar.1999.6248

Hayne PO et al (2017) Global regolith thermophysical properties of the Moon from the Diviner Lunar Radiometer Experiment. J Geophys Res (Planets) 122:2371–2400. https://doi.org/10.1002/2017JE005387

Johnson JB, Kulchitsky AV, Duvoy P, Iagnemma K, Senatore C, Arvidson RE, Moore J (2015) Discrete element method simulations of Mars Exploration Rover wheel performance. Journal of Terramechanics 62:31–40

Jop P, Forterre Y, Pouliquen O (2006) A constitutive law for dense granular flows. Nature 441:727–730

Kawakatsu Y, Kuramoto K, Ogawa N, Ikeda H, Ono G, et al. (2019) Mission definition of Martian moon exploration (MMX). In: 70th international astronautical congress, IAC-19-A3.4.B7, Washington DC, 21-25 Oct 2019

Kessler E (2005) Proceedings of sensor 2005 12th international conference, Vol. I, Nürnberg, pp 73-78

Ksanfomality LV et al (1989) Spatial variations in thermal and albedo properties of the surface of Phobos. Nature 341:588–591. https://doi.org/10.1038/341588a0

Kuehrt E, Giese B, Keller HU, Ksanfomality LV (1992) Interpretation of the KRFM-infrared measurements of Phobos. Icarus 96:213–218. https://doi.org/10.1016/0019-1035(92)90075-I

Kuramoto K et al (2021) Martian moons exploration MMX: sample return mission to Phobos elucidating formation processes of habitable planets. Earth Planets Space. https://doi.org/10.1186/s40623-021-01545-7

Kuzmin RO, Zabalueva EV (2003) The temperature regime of the surface layer of the Phobos regolith in the region of the potential. Solar Syst Res 37:480–488. https://doi.org/10.1023/B:SOLS.0000007946.02888.bd

Lagerros JSV (1996) Thermal physics of asteroids. I. Effects of shape, heat conduction and beaming. Astrono Astrophys 310:1011–1020

Lauretta DS and the OSIRIS-REx TAG Team (2021) The OSIRIS-REx touch-and-go sample acquisition event and implications for the nature of the returned sample. Paper presented at the 52nd lunar and planetary science conference 2021, (LPI Contrib. No. 2548)

Lebofsky LA, Rieke GH (1979) Thermal properties of 433 Eros. Icarus 40:297–308. https://doi.org/10.1016/0019-1035(79)90074-5

Lorenz RD (2020) How far is far enough? Requirements derivation for planetary mobility systems. Adv Space Res 65:1383–1401

Lunine JI, Neugebauer G, Jakosky BM (1982) Infrared observations of Phobos and Deimos from Viking. J Geophys Res 87:10297–10305. https://doi.org/10.1029/JB087iB12p10297

Maimone M, Cheng Y, Matthies L (2007) Two years of visual odometry on the Mars exploration rovers. J Field Robot 24:169–186. https://doi.org/10.1002/rob.20184
Michel P, Ballouz RL, Barnouin OS, Jutzi M, Walsh KJ, May BH, Manzoni C, Richardson DC, Schwartz SR, Sugita S et al (2020) Collisional formation of top-shaped asteroids and implications for the origins of Ryugu and Bennu. Nat Commun 11:1–11. https://doi.org/10.1038/s41467-020-16433-z
Miyamoto H et al (2021) Surface environment of Phobos and Phobos simulant UTPS. Earth Planets Space. https://doi.org/10.1186/s40623-021-01406-3
Müller TG et al (2017) Hayabusa-2 mission target asteroid 162173 Ryugu (1999 JU_3): searching for the object's spin-axis orientation. Astron Astrophys 599:A103. https://doi.org/10.1051/0004-6361/201629134
Mueller NT et al (2020) Calibration of the HP^3 radiometer on InSight. Earth Space Sci 7(5):e01086. https://doi.org/10.1029/2020EA001086
Murdoch N, Sanchez P, Schwartz SR, Miyamoto H (2015) Asteroid surface geophysics. In: Michel P et al (eds) Asteroids IV. University of Arizona, Tucson, pp 767–792. https://doi.org/10.2458/azu_uapress_9780816532131-ch039
Nakamura T et al (2021) Science operation plan of Phobos and Deimos from the MMX spacecraft. Earth Planets Space. https://doi.org/10.1186/s40623-021-01546-6
Nakashima H, Fujii H, Oida A, Momozu M, Kawase Y, Kanamori H, Aoki S, Yokoyama T (2007) Parametric analysis of lugged wheel performance for a lunar microrover by means of DEM. J Terramechanics 44:153–162
Ogawa K, Hamm M, Grott M, Sakatani N, Knollenberg J, Biele J (2019) Possibility of estimating particle size and porosity on Ryugu through MARA temperature measurements. Icarus 333:318–322. https://doi.org/10.1016/j.icarus.2019.06.014
Pieters CM, Murchie S, Thomas N, Britt D (2014) Composition of surface materials on the moons of Mars. Planet Space Sci 102:144–151. https://doi.org/10.1016/j.pss.2014.02.008
Reina G, Ojeda L, Milella A, Borenstein J (2006) Wheel slippage and sinkage detection for planetary rovers. IEEE/ASME Trans Mechatron 11:185–195. https://doi.org/10.1109/TMECH.2006.871095
Rozitis B, et al. (2019) Thermal inertia maps of (101955) Bennu from OSIRIS-REx infrared observations. EPSC-DPS Joint Meeting 2019
Sánchez P, Scheeres DJ (2014) The strength of regolith and rubble pile asteroids. Meteorit Planet Sci 49:788–811
Sedlmayr HJ, Barthelmes S, Bayer R, Bertleff W, Bihler M, Buse F, Chalon M, Franke D, Ginner F, Langofer V, Lichtenheldt R, Obermeier T, Pignède A, Reill J, Skibbe J, Tardivel S (2020) MMX—Development of a rover locomotion system for Phobos. In: IEEE aerospace conference 2020, pp 1–10. https://doi.org/10.1109/AERO47225.2020.9172659
Smith NM, Edwards CS, Mommert M, Trilling DE, Glotch TD (2018) Mapping the thermal inertia of Phobos using MGS-TES observations and thermophysical modelling. In: 49th lunar and planetary science conference, The Woodlands, 19-23 Mar 2018
Spohn T, Seiferlin K, Hagermann A, Knollenberg J, Ball AJ, Banaszkiewicz M, Benkhoff J, Gadomski S, Gregorczyk W, Grygorczuk J, Hlond M, Kargl G, Kuehrt E, Kömle N, Krasowski J, Marczewski W, Zarnecki JC (2007) Mupus - A Thermal and Mechanical Properties Probe for the Rosetta Lander Philae. Space Science Review 128:339–362. https://doi.org/10.1007/s11214-006-9081-2
Spohn T, Knollenberg J, Ball AJ, Banaszkiewicz M, Benkhoff J, Grott M, Grygorczuk J, Hüttig C, Hagermann A, Kargl G, Kaufmann E, Kömle N, Kuehrt E, Kossacki KJ, Marczewski W, Pelivan I, Schrödter R, Seiferlin K (2015) Thermal and mechanical properties of the near-surface layers of comet 67P/Churyumov-Gerasimenko. Science 349:6247. https://doi.org/10.1126/science.aab0464
Spohn T et al (2018) The heat flow and physical properties package (HP^3) for the InSight mission. Space Sci Rev 214:P24D-01
Sullivan R, Anderson R, Biesiadecki J, Bond T, Stewart H (2011) Cohesions, friction angles, and other physical properties of Martian regolith from Mars Exploration Rover wheel trenches and wheel scuffs. J Geophys Res 116:E02006. https://doi.org/10.1029/2010JE003625
Sunday C, Murdoch N, Tardivel S, Schwartz SR, Michel P (2020) Validating N-body code CHRONO for granular DEM simulations in reduced-gravity environments. Mon Not R Astron Soc 498:1062–1079
Thomas PC, Veverka J, Sullivan R et al (2000) Phobos: regolith and ejecta blocks investigated with Mars Orbiter Camera images. J Geophys Res 105:15091–15106
Thomas N, Stelter R, Ivanov A, Bridges NT, Herkenhoff KE, McEwen AS (2011) Spectral heterogeneity on Phobos and Deimos: HiRISE observations and comparisons to Mars Pathfinder results. Planet Space Sci 59:1281–1292. https://doi.org/10.1016/j.pss.2010.04.018
Ulamec S, Michel P, et al. (2019), A rover for the MMX mission to Phobos. In: 70th international astronautical congress, Washington DC, 21–25 Oct 2019
Valette R, Riber S, Sardo L, Castellani R, Costes F, Vriend N, Hachem E (2019) Sensitivity to the rheology and geometry of granular collapses by using the μ(I) rheology. Comput Fluids 191:104260
Vo TT, Nezamabadi S, Mutabaruka P, Delenne JY, Radjai F (2020) Additive rheology of complex granular flows. Nat Commun 11:1476
Wählisch M, Stooke PJ, Karachevtseva IP, Kirk R, Oberst J, Willner K, Nadejdina IA, Zubarev AE, Konopikhin AA, Shingareva KB (2014) Phobos and Deimos cartography. Planet Space Sci 102:60–73. https://doi.org/10.1016/j.pss.2013.05.012
Zhang Y, Lin DNC (2020) Tidal fragmentation as the origin of 1I/2017 U1 ('Oumuamua). Nat Astron 4:852–860

Publisher's Note